J Mater Sci (2011) 46:6491–6499
DOI 10.1007/s10853-011-5595-4

Dissimilar joining of Al/Mg light metals by compound casting process

E. Hajjari · M. Divandari · S. H. Razavi · S. M. Emami · T. Homma · S. Kamado

Received: 7 April 2011 / Accepted: 26 April 2011 / Published online: 7 May 2011

Abstract "Compound casting" was used for production of lightweight Al/Mg couples. In order to prepare the Al/Mg couples using this process, each of the aluminum and magnesium molten metal was cast around solid cylindrical inserts of the other metal. After solidification, the interfacial microstructure and shear strength of the joint were studied. Characterization of Al/Mg interface by an optical microscope and scanning electron microscope showed that in the case of casting aluminum melt around a magnesium insert, a gap is formed at the interface, while in the process of casting magnesium melt around an aluminum insert, a relatively uniform interface composed of three different layers is formed at the interface. The results of the X-ray diffraction, energy dispersive X-ray spectroscopy, wavelength dispersive X-ray spectroscopy, and microhardness analysis of the interface showed that these three layers are mainly composed of high-hardness Al–Mg intermetallic compounds. Furthermore, it was found that the thickness of the interface is not constant throughout Al/Mg joint, and varies gradually from 190 μm at the bottom to 140 μm in the middle and 50 μm at the top of the sample. The results of shear strength tests obviously showed that the strength of the interface depends on the interface thickness and increases by decreasing the thickness of the interface.

E. Hajjari (✉) · M. Divandari · S. H. Razavi · S. M. Emami
Department of Metallurgy and Materials Engineering, Iran University of Science and Technology, Tehran 16846-13114, Iran
e-mail: e_hajjari@iust.ac.ir

T. Homma · S. Kamado
Department of Mechanical Engineering, Nagaoka University of Technology, Nagaoka 940-2188, Japan

Introduction

Magnesium and aluminum are the first and second engineering light metals, respectively, and are attractive in vehicle structure applications for improving energy efficiency, which reduces the emission of greenhouse gases. In many cases, one of these materials alone does not satisfy the requirements of lightweight constructions, and dissimilar joining between these two metals must be faced. A variety of attempts have been dedicated to joining Al/Mg alloys using different fusion welding and solid-state joining methods such as tungsten inert gas welding [1], laser welding [2–4], friction-stir welding (FSW) [5–7], and vacuum diffusion bonding [8, 9]. The major problem in these joining processes is the formation of much more Al–Mg intermetallic compounds with a very high hardness and brittleness between aluminum and magnesium as an interlayer, which is deleterious to the mechanical properties. However, solid-state joining processes such as FSW and vacuum diffusion bonding can achieve relatively higher joining strengths compared to fusion methods, due to elimination of defects like shrinkage porosities and inclusions, for the direct contact between aluminum and magnesium base metals, there are also Al–Mg intermetallic compounds in the joints [6, 10]. In addition, long process time and high corresponding operating cost of the vacuum diffusion bonding and specific requirements for the shape of the substrate in FSW may render these solid-state joining processes not easy for practical and industrial applications.

Compound casting is a process through which two metallic materials—one in solid state and the other liquid—are brought into contact with each other. In this way, a diffusion reaction zone between the two materials and thus a continuous metallic transition from one metal to

the other is formed [11]. This method could join semi-finished parts with complex structures, simply by casting a metal onto or around a solid shape. However, many researchers have used compound casting to join different similar and dissimilar metallic couples such as steel/cast iron [12, 13], steel/Cu [14], steel/Al [15, 16], Cu/Al [17], Al/Al [15, 18, 19], and Mg/Mg [20], joining dissimilar light metals such as aluminum and magnesium by the compound casting process is still a relatively unexplored area. In this study, compound casting as an economic straightforward in situ technique was used to join dissimilar aluminum and magnesium light metals. Joint conditions including microstructure characteristics and mechanical properties were examined in order to find a new way to join Al/Mg dissimilar materials and lay a foundation for the practical use of these light-metal joints.

Experimental procedures

Materials

Commercially pure aluminum and commercially pure magnesium were used to prepare the Al/Mg couples by the compound casting process. Chemical compositions of the materials used are listed in Table 1.

Casting process

In order to fabricate the Al/Mg couples by the compound casting process, cylindrical inserts with 20 mm diameter and 100 mm height were machined from aluminum and magnesium ingots. Their surfaces were ground with silicon carbide papers up to 1200 grit, then rinsed with acetone and placed within a cylindrical cavity of a CO_2 sand mold with 30 mm diameter and 80 mm height. Two series of samples were prepared. In the first series, aluminum ingots were melted in a clay-graphite crucible placed in an electrical resistance furnace. The molten aluminum was cast around the magnesium inserts at 700 °C under normal atmospheric conditions. In the second series, magnesium ingots were melted in a steel crucible placed in the same furnace under the Foseco MAGREX 36 covering flux, to protect magnesium melt form oxidation. The molten magnesium was cast around the aluminum inserts at 700 °C under normal atmospheric conditions. Schematic sketches of the mold used in the casting process and the prepared Al/Mg couple are illustrated in Fig. 1.

Table 1 Chemical compositions (wt%) of the materials used in this study

Material	Al	Si	Fe	Cu	Mn	Mg	Zn	Sn
Al[a]	Bal.	0.131	0.171	0.002	0.009	0.027	0	0.076
Mg[b]	0	0.029	0.002	0.012	0.017	Bal.	0.093	0

[a] Commercially pure aluminum

[b] Commercially pure magnesium

Microstructural evaluations

In order to study the interfacial microstructure of the Al/Mg couples in the compound casting process, specimens were cut from the bottom, middle, and top parts of the samples perpendicular to the cylindrical insert, using an electrical discharge machine (Fig. 1b), and were prepared with a final oxide polish (OP-S). Owing to nature of dissimilar metals bond, specimens were etched by a 1% HF distilled water solution on the aluminum side and a 1% HNO_3 alcohol solution on the magnesium side. Specimens were examined using an Olympus BX51M optical microscope and a JEOL JSM-7000F scanning electron microscope (SEM) equipped with the energy dispersive X-ray spectroscopy (EDS) and wavelength dispersive X-ray spectroscopy (WDS) detectors. The phase constitutions on the fracture surfaces of the specimens were also identified by using a Rigaku RINT-RAPID X-ray diffractometer.

Mechanical characterizations

Mechanical characterizations of the Al/Mg joint were conducted for the samples prepared by casting magnesium melt around the aluminum insert, using microhardness and

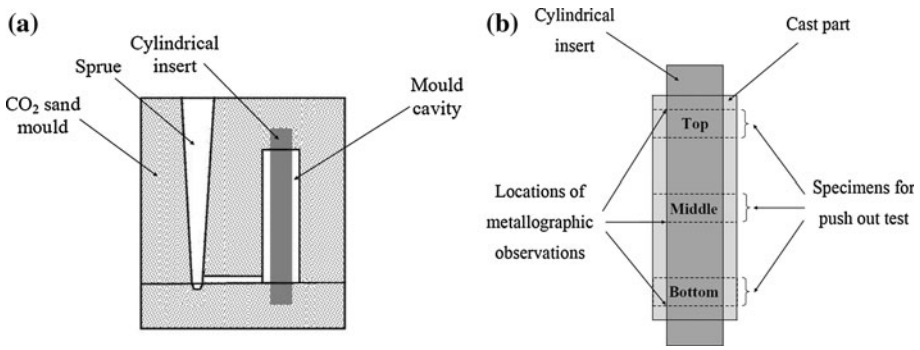

Fig. 1 Schematic sketches of **a** the mold used for the casting process and **b** the prepared Al/Mg couple

push-out tests. A Mitutoyo hardness tester with a testing load of 10 g and a holding time of 15 s was used to determine the Vickers micro hardness profile across the joint interface.

In order to determine the shear strength of the Al/Mg interface, slices with a thickness of 10 mm were cut from the bottom, middle, and top parts of the samples perpendicular to the cylindrical insert using an electrical discharge machine (Fig. 1b). The tests were performed by using a Shimadzu AG-I 50 kN electronic universal testing machine. The specimens were put on a flat supporting surface with a circular hole of 22 mm diameter and pushed by means of a steel cylinder stub punch, concentric with the support hole, with an 18 mm diameter at a cross-head displacement rate of 0.2 mm min^{-1}. At least three slices from each part of the sample were submitted to push-out test. Shear strength of the interface (τ_{int}) was calculated using the following equation [21, 22]:

$$\tau_{int} = \frac{F_{max}}{2\pi rt} \quad (1)$$

where F_{max} is the maximum load, r is the insert radius (10 mm), and t is the specimen thickness (10 mm). A schematic sketch of the setup used for the push-out tests is illustrated in Fig. 2.

Results and discussion

Microstructures

The optical micrographs in Figs. 3 and 4 show the typical interfacial microstructures of the Al/Mg joints in the compound casting process. Figure 3a, b, and c are related to the bottom, middle, and top parts of a sample prepared by casting aluminum melt around a magnesium insert, respectively. Figure 4a, b, and c are related to the same parts of a sample prepared by casting magnesium melt around an aluminum insert, respectively. Figure 5 shows SEM micrographs from the same parts of the sample shown in Fig. 4. A typical EDS map of the elements Al, Mg, and O is shown in Fig. 6. This map scan refers to the SEM micrograph shown in Fig. 5b.

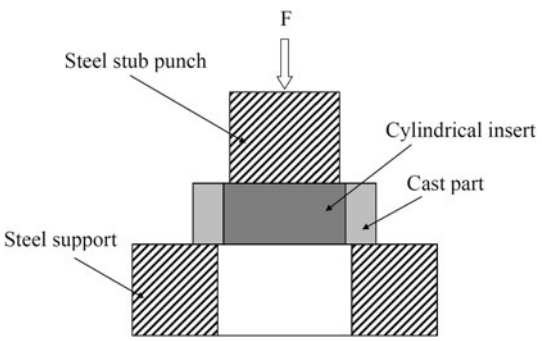

Fig. 2 Schematic sketch of the setup used for push-out tests

As can be seen in Fig. 3, after casting aluminum melt around a magnesium insert, in almost all parts of the sample a relatively large gap has been formed at the interface and only some local and limited interactions in different parts of the interface have occurred due to contact between the aluminum melt and magnesium insert. As shown in Fig. 4, in casting magnesium melt around the aluminum insert, a relatively uniform interface has been formed due to contact between the magnesium melt and aluminum insert. In this case, there is no macroscopic crack at the joint, but a few holes existed at the interface layer owing to gas and/or shrinkage porosities.

From thermodynamic viewpoint, owing to the negative standard Gibbs free energy, the magnesium melt can react with the thin aluminum oxide layer on the surface of the aluminum insert, and reduce it according to reaction below [23]:

$$\begin{aligned} &Mg_{(l)} + 1\big/3Al_2O_{3(s)} \rightarrow MgO_{(s)} + 2\big/3Al_{(l)} \\ &\Delta G^0 = -39 kJ\,mol^{-1} \text{ of Mg at } 1000\,K \end{aligned} \quad (2)$$

In addition further reaction between the produced magnesium oxide and the oxide layer on the surface of the aluminum insert can result in formation of the spinel ($MgO{\cdot}Al_2O_3$) as follow [23]:

$$\begin{aligned} &MgO_{(s)} + Al_2O_{3(s)} \rightarrow MgO \cdot Al_2O_{3(s)} \\ &\Delta G^0 = -30\,kJ\,mol^{-1} \text{ of MgO at } 1000\,K \end{aligned} \quad (3)$$

This can bring about removing the oxide layer from the surface of the aluminum insert and thus direct contact between the fresh aluminum insert surface and magnesium melt, and lead to formation of an interfacial layer between them. On the other hand, because of the positive standard Gibbs free energy for the reaction (2) in the opposite direction, the aluminum melt is not capable to react with the magnesium oxide on the surface of the magnesium insert to reduce it. Therefore, after contact between the aluminum melt and magnesium insert, a gap is formed within the interface. Furthermore, based on the difference in mean coefficient of thermal expansion (CTE) for magnesium ($25.5 \times 10^{-6}\ K^{-1}$) and aluminum ($24 \times 10^{-6}\ K^{-1}$) [24], the contraction during cooling from the liquidus to the room temperature for magnesium is more than that for aluminum (1.6% for magnesium vs. 1.4% for aluminum). This can bring about tightening of the interface when casting magnesium melt around an aluminum insert, and loosening when casting aluminum melt around a magnesium insert.

Considering the micrographs in Figs. 4 and 5, when the magnesium melt is cast around the aluminum insert, the interfacial microstructure of the Al/Mg joint consists of three different layers. According to the EDS map in Fig. 6,

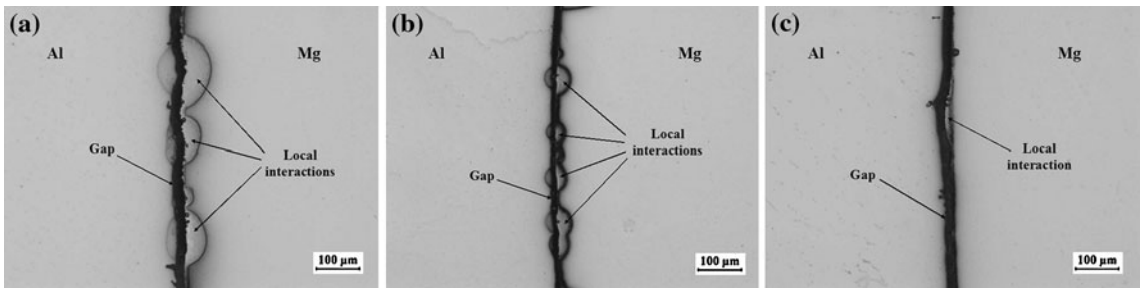

Fig. 3 Optical micrographs of interfacial microstructures from different parts of the Al/Mg joint in the compound casting process in the case of casting aluminum melt around a magnesium insert; **a** bottom, **b** middle, and **c** top

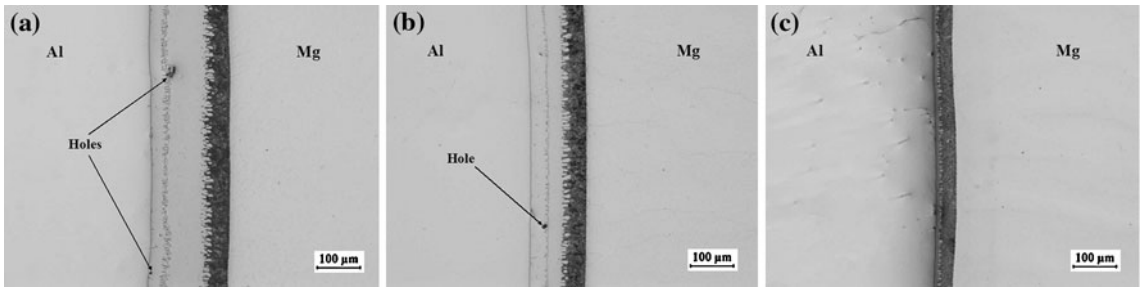

Fig. 4 Optical micrographs of interfacial microstructures from different parts of the Al/Mg joint in the compound casting process in the case of casting magnesium melt around an aluminum insert; **a** bottom, **b** middle, and **c** top

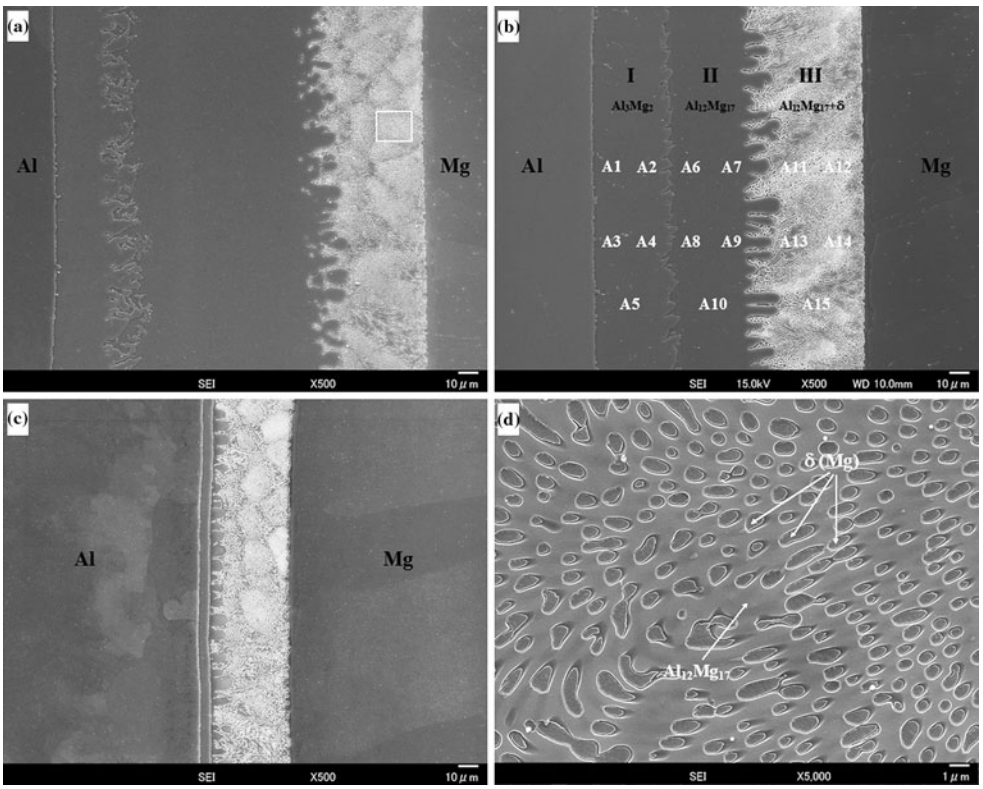

Fig. 5 SEM micrographs of interfacial microstructures from different parts of the Al/Mg joint in the compound casting process in the case of casting magnesium melt around an aluminum insert; **a** bottom, **b** middle, **c** top, and **d** marked area in **a**

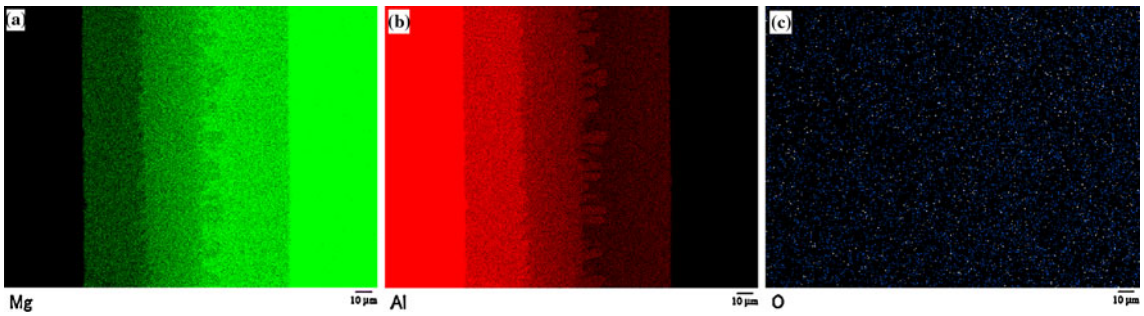

Fig. 6 EDS map from cross section of the Al/Mg joint in the compound casting process when casting magnesium melt around the aluminum insert corresponding to the SEM micrograph shown in Fig. 5b; **a** magnesium distribution map, **b** aluminum distribution map, and **c** oxygen distribution map

it can be deduced that the layers adjacent to the aluminum and magnesium base metals in Fig. 5b are rich in aluminum and magnesium, respectively. In addition, a concentration gradient of aluminum and magnesium elements can be seen at the middle layer, while no oxygen concentration was detected at any part of the interface.

Formation of the different layers with different compositions between the aluminum insert and magnesium melt implies that diffusion is the dominant mechanism for mass transportation in the compound casting process, as is the case with solid-state diffusion bonding. During this process, the heat of the melt causes the surface layer of the cylindrical insert to be melted, and then concentration gradients cause the aluminum and magnesium melts to diffuse into each other. After that, according to the Al–Mg binary phase diagram (Fig. 7), intermetallic compounds such as Al_3Mg_2 and $Al_{12}Mg_{17}$ can be formed within the interface after finishing the solidification.

X-ray diffraction patterns of the constitutive phases on the fracture surfaces of the Al/Mg joint prepared by casting magnesium melt around the aluminum insert (Fig. 8) confirm the formation of the Al_3Mg_2 and $Al_{12}Mg_{17}$ intermetallic compounds within the interface microstructure.

Quantitative analysis results of aluminum and magnesium elements by WDS in fifteen different areas (A1–A15 in Fig. 5b) of the interface between the aluminum insert and magnesium melt are listed in Table 2.

These results imply that the layer on the aluminum side (layer I) is mainly composed of the Al_3Mg_2 intermetallic compound, while the $(Al_{12}Mg_{17} + \delta)$ eutectic structure

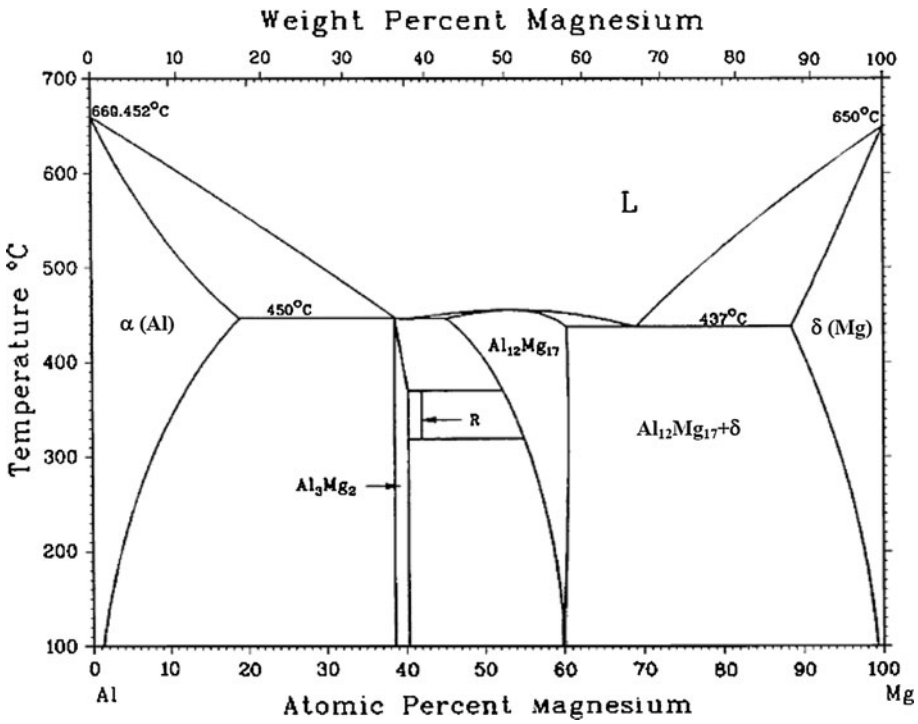

Fig. 7 Al–Mg binary phase diagram [25]

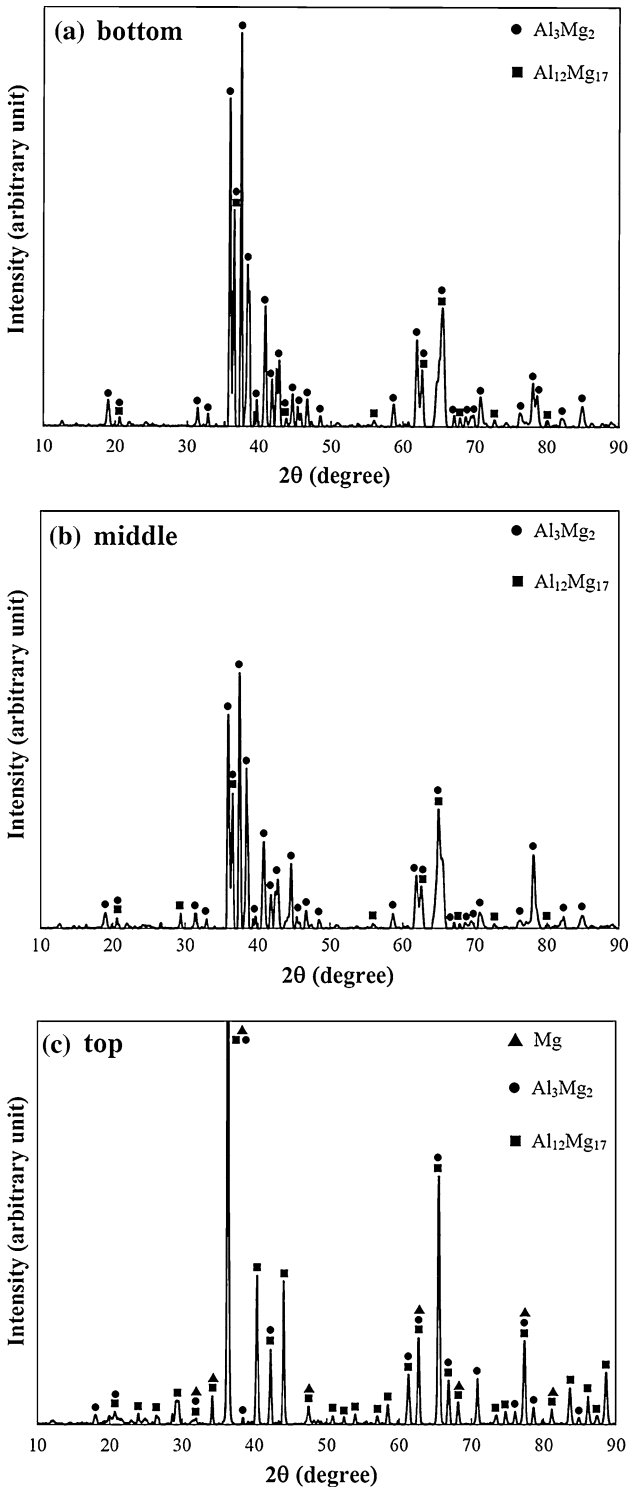

Fig. 8 XRD patterns of the constitutive phases on the fracture surfaces of the Al/Mg joint in different parts of the sample prepared by casting magnesium melt around an aluminum insert; **a** bottom, **b** middle, and **c** top

due to the $L \xrightarrow{437\,^{\circ}C} Al_{12}Mg_{17} + \delta$ eutectic transformation is the main constituent of the layer on the magnesium side (layer III). The SEM micrograph shown in Fig. 5d confirms

Table 2 WDS quantitative analysis results of aluminum and magnesium elements at the Al/Mg interface

Area number	Layer code	Element compositions (at.%)		Element compositions ratio (Al:Mg)	Inference component
		Al	Mg		
A1	I	59.877	40.123	1.492	Al_3Mg_2
A2		59.524	40.476	1.470	Al_3Mg_2
A3		60.315	39.685	1.519	Al_3Mg_2
A4		59.319	40.681	1.458	Al_3Mg_2
A5		60.308	39.692	1.519	Al_3Mg_2
A6	II	49.306	50.694	0.974	$Al_{12}Mg_{17}$
A7		41.463	58.537	0.708	$Al_{12}Mg_{17}$
A8		48.764	51.236	0.952	$Al_{12}Mg_{17}$
A9		42.402	57.598	0.736	$Al_{12}Mg_{17}$
A10		45.885	54.115	0.848	$Al_{12}Mg_{17}$
A11	III	24.441	75.559	0.323	$Al_{12}Mg_{17} + \delta$
A12		28.577	71.423	0.400	$Al_{12}Mg_{17} + \delta$
A13		29.585	70.415	0.420	$Al_{12}Mg_{17} + \delta$
A14		28.075	71.925	0.390	$Al_{12}Mg_{17} + \delta$
A15		25.812	74.188	0.348	$Al_{12}Mg_{17} + \delta$

δ is magnesium solid solution

the formation of the rod-like ($Al_{12}Mg_{17} + \delta$) eutectic structure in the layer III. In the case of layer II, unlike layers I and III which almost have constant chemical compositions, the ratio of aluminum and magnesium for different areas of the layer is not constant and varies from 0.708 to 0.974. Considering the relatively wide range of the composition for the $Al_{12}Mg_{17}$ intermetallic compound in the Al–Mg binary phase diagram (45–60 at.% Mg) shown in Fig. 7, it seems that the middle layer (layer II) is mainly composed of the $Al_{12}Mg_{17}$ intermetallic compound.

As a result, according to the micrographs shown in Figs. 4 and 5, the whole thickness of the interface at different heights of the sample is not constant, and varies from about 190 μm at the bottom to 140 μm in the middle and 50 μm at the top of the sample. The decrease in the interface thickness from the bottom to top of the sample seems to be due to the cooling effect of the aluminum insert and also difference in the hydrostatic pressure of the magnesium melt at different heights of the mold. During filling the mold with the magnesium melt, contact between the solid aluminum insert and magnesium melt gradually brings about a decrease in the total heat content of the melt. Therefore, surface melting of the aluminum insert due to contact with the magnesium melt decreases from bottom to top, which causes a gradual decrease in the total thickness of the interface from the bottom to top of the sample. Furthermore, the hydrostatic pressure of the magnesium melt at the bottom of the mold is greater than those for the middle and top parts of it. This can lead to the better contact between the

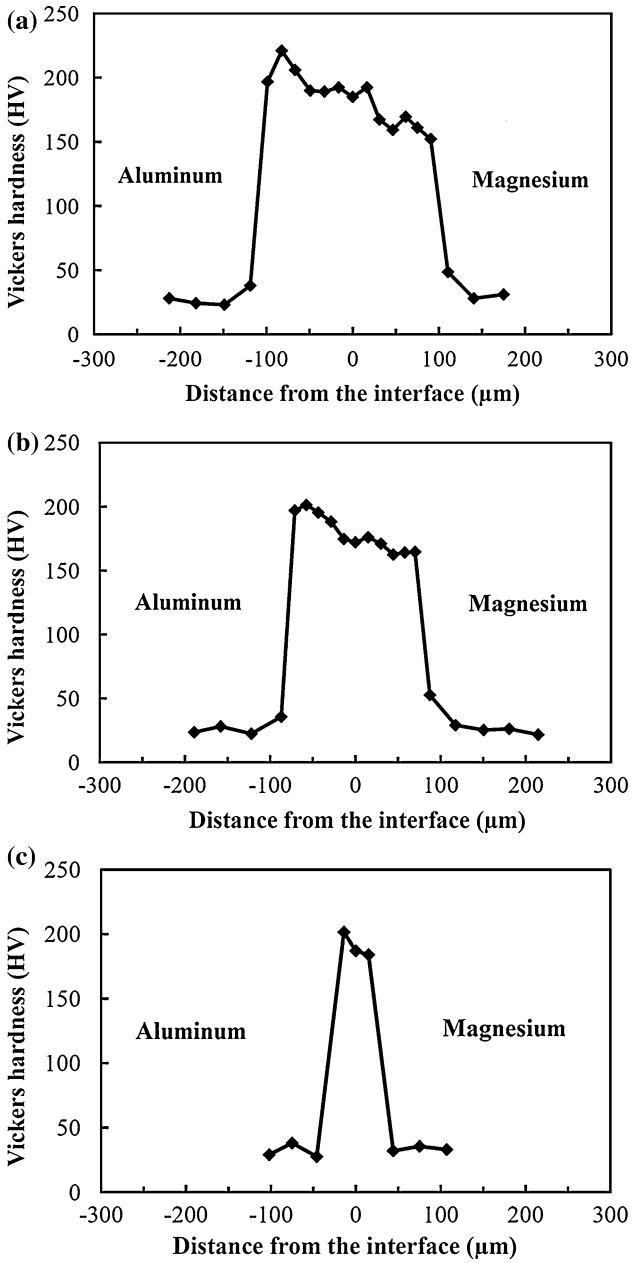

Fig. 9 Microhardness distributions from the interface zone at different parts of the Al/Mg joint prepared by casting magnesium melt around the aluminum insert (referring to the micrographs shown in Figs. 4 and 5); **a** bottom, **b** middle, and **c** top

aluminum insert and magnesium melt at an earlier stage at the bottom of the mold, and thus longer period for interdiffusion of the components which can consequently bring about thicker interface at the bottom of the sample compared to its middle and top parts. On the other hand, as can be seen in Figs. 4 and 5, the major part of the decrease in the interface thickness at the top part of the sample concerns layers I and II, and the thickness of layer III is almost constant at different parts of the Al/Mg joint. This means that the formation of layer III occurs at the early stage of the contact between the aluminum insert and magnesium melt due to diffusion of aluminum element into the magnesium melt. Subsequently with further diffusion of the aluminum and magnesium elements into each other, layers II and I are formed and start to grow within the interface.

Table 3 Shear strength of different parts of the Al/Mg joint prepared by the compound casting process

Sample position	Thickness of the interface (μm)	Test number	Maximum shear load (kN)	Shear strength (MPa)	Average shear strength (MPa)
Top	50	1	23.2	37.0	39.9
		2	26.3	41.9	
		3	25.6	40.7	
Middle	140	1	18.3	29.1	27.1
		2	15.9	25.3	
		3	16.9	26.9	
Bottom	190	1	12.1	19.3	20.2
		2	14.6	23.2	
		3	11.4	18.2	

Mechanical properties

Microhardness distributions from the interface zone at the bottom, middle, and top parts of the Al/Mg joint prepared by casting magnesium melt around the aluminum insert are shown in Fig. 9.

As can clearly be seen in this figure, the microhardness distributions are consistent with the microstructures of the interface shown in Figs. 4 and 5. For all the bottom, middle, and top parts of the joint, the hardness of the interface is significantly higher than those of the aluminum and magnesium base metals. The microhardness ranges from HV 152 to HV 221 depending on the location in the interface, while the base metals of aluminum and magnesium have average hardness values of HV 25 and HV 28, respectively. Noticeable higher hardness of the interface than of the aluminum and magnesium base metals confirms that the high-hardness Al–Mg intermetallic compounds have been formed within the Al/Mg interface. Moreover, according to Fig. 9, the microhardness of the interface at the aluminum side (layer I) is higher than that of the magnesium side (layer III) and the intermediate area (layer II), which means the Al_3Mg_2 intermetallic compound has higher hardness than the $Al_{12}Mg_{17}$ intermetallic compound and the $(Al_{12}Mg_{17} + \delta)$ eutectic structure. This is in agreement with the reports from Liu et al. [1] and Dietrich et al. [26].

The results of push-out shear strength tests obtained at different parts of the Al/Mg joint are shown in Table 3.

The average shear strength of the interface increases from 20.2 to 27.1 and 39.9 MPa at the bottom, middle, and

top parts of the joint, respectively. This indicates that the shear strength for the top part of the joint is considerably higher than those for the middle and bottom parts. The maximum shear strengths of the Al/Mg joint in the laser welding and diffusion bonding processes have been reported as 48 [2] and 83 MPa [10], respectively. Change in the shear strength of the interface from the bottom to top of the joint prepared by the compound casting process seems to result from different thicknesses of the interface. Since the interface of the Al/Mg joint is mainly composed of high-hardness intermetallic compounds, a decrease in its thickness can cause an increase in the joint strength.

Figure 10 shows the fracture surfaces of the Al/Mg joint in different parts of the sample in the compound casting process. The fractures are mostly brittle, but the fracture surfaces of the bottom and middle parts of the sample (Fig. 10a–d) are obviously flatter than seen in the top part (Fig. 10e, f). The presence of beach marks on some parts of the fracture surface of the Al/Mg joint in the top of the sample indicates a partly ductile fracture for this part of the joint.

Based on the XRD results (Fig. 8), for all parts of the sample the failure has occurred at the intermetallic compounds within the interface, which seems to be caused by the high hardness and brittleness of the Al–Mg intermetallic compounds. According to the XRD results (Fig. 8), the dominant intermetallic compound on the fracture surfaces of the Al/Mg joint on the bottom and middle parts of the sample is Al_3Mg_2. Meanwhile for the top part of the sample, $Al_{12}Mg_{17}$ is the dominant intermetallic compound on the fracture surface.

It seems that as a consequence of higher hardness and lower plastic deformability, the fracture of the sample at the bottom and middle parts occurs primarily in the Al_3Mg_2 intermetallic compound. However, for the top part of the sample, given the very low thickness of the layers containing the Al_3Mg_2 and $Al_{12}Mg_{17}$ intermetallic compounds (layers I and II), the fracture mainly occurs within the $(Al_{12}Mg_{17} + \delta)$ eutectic structure (layer III), resulting in different fracture morphology and higher shear strength for this part of the joint. Secondary δ phases shown by arrows on the fracture surface of the Al/Mg joint in the top part of the sample (Fig. 10f) indicate that the fracture has occurred from within the $(Al_{12}Mg_{17} + \delta)$ eutectic structure (layer III).

Conclusions

a) Joining of aluminum and magnesium by the compound casting process is possible only via casting magnesium melt around the aluminum insert, while in the case of casting aluminum melt around the magnesium insert, a gap is formed at the interface due to presence of oxide layers on the surface of the aluminum melt and magnesium insert and also because of the interface loosening, caused by higher CTE of the magnesium insert than the cast aluminum.

b) Formation of the interface in the compound casting process is diffusion controlled and the interface consists of three different layers. The layers adjacent

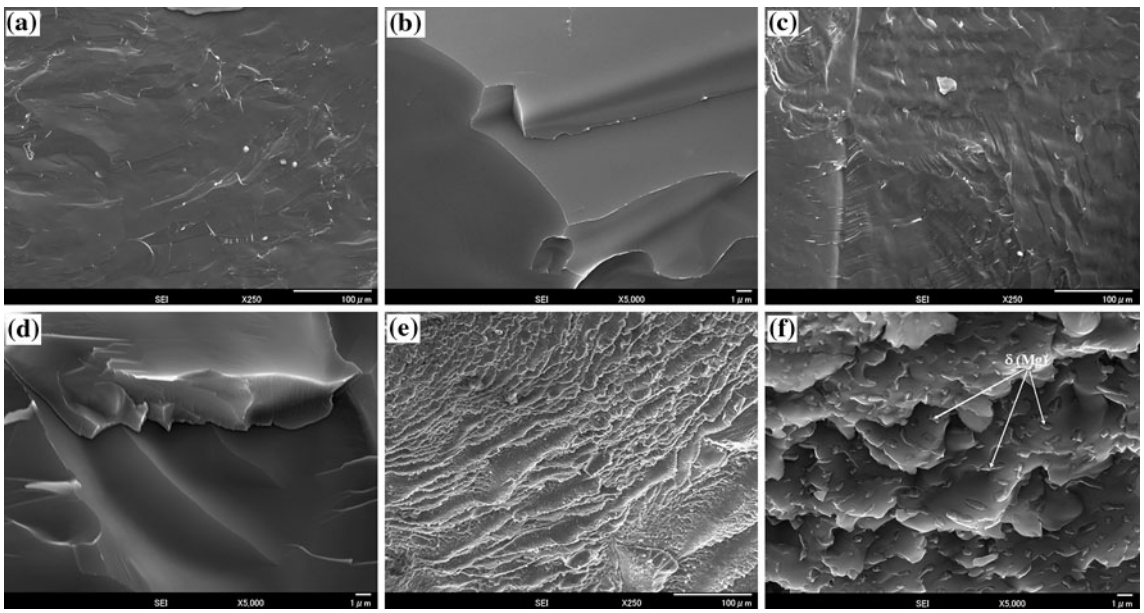

Fig. 10 Fracture surfaces of different parts of the Al/Mg joint in the compound casting process; **a**, **b** bottom part, brittle fracture in the Al_3Mg_2 intermetallic compound, **c**, **d** middle part, brittle fracture in the Al_3Mg_2 intermetallic compound, and **e**, **f** top part, partly ductile fracture in the $(Al_{12}Mg_{17} + \delta)$ eutectic structure

to the aluminum and magnesium base metals are composed of the Al_3Mg_2 intermetallic compound and the $(Al_{12}Mg_{17} + \delta)$ eutectic structure, respectively, and the middle layer is composed of the $Al_{12}Mg_{17}$ intermetallic compound.

c) Gradual decrease in the total heat content of the melt during the casting process and also the difference in the hydrostatic pressure of the magnesium melt at different heights of the mold cause a change in interface thickness for different parts of the joint. The maximum and minimum thicknesses achieved in this study are 190 and 50 μm which correspond to the bottom and top of the joint, respectively.

d) Shear strength of the interface is fairly dependent on the interface thickness and varied from 20.2 MPa at the bottom to 39.9 MPa at the top of the joint.

Acknowledgements The authors would like to thank Messrs. T. Ishihara and F. Uchida for technical assistance in characterization of the samples. The first author also acknowledges the Iran Ministry of Science, Research, and Technology and Shahid Chamran University of Ahwaz for financial support.

References

1. Liu P, Li Y, Geng H, Wang J (2007) Mater Lett 61:1288
2. Borrisutthekul R, Miyashita Y, Mutoh Y (2005) Sci Tech Adv Mater 6:199
3. Liu LM, Wang HY, Zhang ZD (2007) Scr Mater 56:473
4. Liu L, Wang H, Song G, Ye J (2007) J Mater Sci 42:565. doi:10.1007/s10853-006-1068-6
5. Zettler R, Augusto A, Silva MD, Rodrigues R, Blanco A, Santos JFD (2006) Adv Eng Mater 8:415
6. Sato YS, Park SHC, Michiuchi M, Kokawa H (2004) Scr Mater 50:1233
7. Yan J, Xu Z, Li Z, Li L, Yang S (2005) Scr Mater 53:585
8. Peng L, Yajiang L, Haoran G, Juan W (2006) Vacuum 80:395
9. Wang J, Yajiang L, Wanqun H (2008) React Kinet Catal 95:71
10. Zhao LM, Zhang ZD (2008) Scr Mater 58:283
11. Volder JP (1993) Aluminium 4:11
12. Noguchi T, Kamota S, Sato T, Sakai M (1993) AFS Trans 89:231
13. Avci A, Ilkaya N, Simsir M, Akdemir A (2009) J Mater Process Technol 209:1410
14. Ho JS, Lin CB, Liu CH (2004) J Mater Sci 39:2473. doi:10.1023/B:JMSC.0000020012.88809.33
15. Pan J, Yoshida M, Sasaki G, Fukunaga H, Fujimura H, Matsuura M (2000) Scr Mater 43:155
16. Choe KH, Park KS, Kang BH, Cho GS, Kim KY, Lee KW, Kim MH, Ikenaga A, Koroyasu S (2008) J Mater Sci Technol 24:60
17. Divandari M, Vahid Golpayegani AR (2009) Mater Des 30:3279
18. Scanlan M, Browne DJ, Bates A (2005) Mater Sci Eng A 413–414:66
19. Papis KJM, Hallstedt B, Loffler JF, Uggowitzer PJ (2008) Acta Mater 56:3036
20. Papis KJM, Loffler JF, Uggowitzer PJ (2010) Mater Sci Eng A 527:2274
21. Sacerdote-Peronnet M, Guiot E, Bosselet F, Dezellus O, Rouby D, Viala JC (2007) Mater Sci Eng A 445–446:296
22. Dezellus O, Milani L, Bosselet F, Sacerdote-Peronnet M, Rouby D, Viala JC (2008) J Mater Sci 43:1749. doi:10.1007/s10853-007-2411-2
23. Reaction-Web, Fact-Web Programs. http://www.crct.polymtl.ca/factweb.php
24. Thermal properties of metals (2002) ASM ready reference, 1st edn. ASM International, Materials Park
25. Alloy phase diagrams (1995) ASM Handbook, vol 3, 9th edn. ASM International, Materials Park
26. Dietrich D, Nickel D, Krause M, Lampke T, Coleman MP, Randle V (2010) J Mater Sci 46:357. doi:10.1007/s10853-010-4841-5